5-2003

Interaction of Tl+ with Product Complexes of Fructose-1,6-bisphosphatase

Jun-yong Choe
Iowa State University

Scott W. Nelson
Iowa State University, swn@iastate.edu

Herbert J. Fromm
Iowa State University

Richard B. Honzatko
Iowa State University, honzatko@iastate.edu

Interaction of Tl+ with Product Complexes of Fructose-1,6-bisphosphatase

Abstract
The dissociation equilibrium constant for heparin binding to antithrombin III (ATIII) is a measure of the cofactor's binding to and activation of the proteinase inhibitor, and its salt dependence indicates that ionic and non-ionic interactions contribute ~40 and ~60% of the binding free energy, respectively. We now report that phenylalanines 121 and 122 (Phe-121 and Phe-122) together contribute 43% of the total binding free energy and 77% of the energy of non-ionic binding interactions. The large contribution of these hydrophobic residues to the binding energy is mediated not by direct interactions with heparin, but indirectly, through contacts between their phenyl rings and the non-polar stems of positively charged heparin binding residues, whose terminal amino and guanidinium groups are thereby organized to form extensive and specific ionic and non-ionic contacts with the pentasaccharide. Investigation of the kinetics of heparin binding demonstrated that Phe-122 is critical for promoting a normal rate of conformational change and stabilizing AT*H, the high affinity-activated binary complex. Kinetic and structural considerations suggest that Phe-122 and Lys-114 act cooperatively through non-ionic interactions to promote P-helix formation and ATIII binding to the pentasaccharide. In summary, although hydrophobic residues Phe-122 and Phe-121 make minimal contact with the pentasaccharide, they play a critical role in heparin binding and activation of antithrombin by coordinating the P-helix-mediated conformational change and organizing an extensive network of ionic and non-ionic interactions between positively charged heparin binding site residues and the cofactor.

Keywords
Biochemistry, Catalysis, Chemical activation, fructose bisphosphatase, hydroxyl group, enzyme kinetics, molecular interaction

Comments
This article is from *Journal of Biological Chemistry* 278 (2003): 16008, doi:10.1074/jbc.M212394200. Posted with permission.

THE JOURNAL OF BIOLOGICAL CHEMISTRY
Vol. 278, No. 18, Issue of May 2, pp. 16008–16014, 2003

Printed in U.S.A.

Interaction of Tl^+ with Product Complexes of Fructose-1,6-bisphosphatase*

Received for publication, December 5, 2002
Published, JBC Papers in Press, February 20, 2003, DOI 10.1074/jbc.M212394200

Jun-Yong Choe, Scott W. Nelson, Herbert J. Fromm, and Richard B. Honzatko‡

From the Department of Biochemistry, Biophysics, and Molecular Biology, Iowa State University, Ames, Iowa 50011

Fructose-1,6-bisphosphatase requires divalent cations (Mg^{2+}, Mn^{2+}, or Zn^{2+}) for catalysis, but a diverse set of monovalent cations (K^+, Tl^+, Rb^+, or NH_4^+) will further enhance enzyme activity. Here, the interaction of Tl^+ with fructose-1,6-bisphosphatase is explored under conditions that support catalysis. On the basis of initial velocity kinetics, Tl^+ enhances catalysis by 20% with a K_a of 1.3 mM and a Hill coefficient near unity. Crystal structures of enzyme complexes with Mg^{2+}, Tl^+, and reaction products, in which the concentration of Tl^+ is 1 mM or less, reveal Mg^{2+} at metal sites 1, 2, and 3 of the active site, but little or no bound Tl^+. Intermediate concentrations of Tl^+ (5–20 mM) displace Mg^{2+} from site 3 and the 1-OH group of fructose 6-phosphate from in-line geometry with respect to bound orthophosphate. Loop 52–72 appears in a new conformational state, differing from its engaged conformation by disorder in residues 61–69. Tl^+ does not bind to metal sites 1 or 2 in the presence of Mg^{2+}, but does bind to four other sites with partial occupancy. Two of four Tl^+ sites probably represent alternative binding sites for the site 3 catalytic Mg^{2+}, whereas the other sites could play roles in monovalent cation activation.

Fructose-1,6-bisphosphatase (FBPase,[1] EC 3.1.3.11) hydrolyzes fructose 1,6-bisphosphate ($F16P_2$) to fructose 6-phosphate (F6P) and phosphate (P_i) (1–6). Fructose 2,6-bisphosphate ($F26P_2$) and AMP synergistically inhibit FBPase. AMP inhibits by way of an allosteric and cooperative mechanism with a Hill coefficient of 2 (7–9). $F26P_2$ competes with $F16P_2$ for the active site (10–12). Coordinated regulation of glycolysis and gluconeogenesis occurs *in vivo*, largely because of opposite effects caused by $F26P_2$ on FBPase (inhibition) and fructose 6-phosphate 1-kinase (activation). Divalent cations (Mg^{2+}, Mn^{2+}, and/or Zn^{2+}) are an absolute requirement for FBPase activity. Enzyme activity increases sigmoidally as a function of divalent cation concentration at pH 7.5 (Hill coefficient of ~2), but at pH 9.6 the variation is hyperbolic (8, 14).

The mammalian enzyme is a homotetramer and exists in distinct conformational states, depending on the relative concentrations of active site ligands and AMP (15). With or without metal cofactors and/or other active site ligands, but in the absence of AMP, FBPase is in its R-state (16, 17). In the presence of AMP, however, the top pair of subunits rotates 17° relative to the bottom pair, resulting in the T-state conformer (18–20). The minimum distance separating AMP molecules from any given active site is ~28 Å (18–20). Yet studies in kinetics, NMR, fluorescence, and x-ray crystallography reveal competition between AMP and divalent cations (11, 20–22).

Loop 52–72 evidently plays a central role in allosteric inhibition of catalysis by AMP. It can be in at least three conformational states: engaged, disordered, and disengaged (17, 20, 23). The engaged conformation is arguably required for the high affinity association of divalent cations and in stabilizing the transition state (17, 23–26). The disordered conformation of the loop may facilitate product release and substrate association. The loop can be in its engaged or disordered conformations in the R-state enzyme. The T-state, however, favors a single (disengaged) conformation for the loop, which cannot stabilize divalent cation association at the active site. Interactions between the loop and residues near the N terminus of an adjacent subunit play an important role in stabilizing the disengaged conformation of the loop (23).

In addition to the absolute requirement for divalent cations, certain monovalent cations (K^+ and Tl^+ among others) further enhance catalysis by FBPase (3, 5, 13). The precise mechanism by which monovalent cations exert their influence, however, has yet to be determined. Monovalent cation activation is in some fashion related to loop 52–72. Mutations of specific residues of the dynamic loop increase the K_a for Mg^{2+}, and without exception also abolish K^+-induced effects on catalysis (25, 26). On the other hand, K^+ does not increase the fraction of subunits with an engaged loop in the presence of saturating Mg^{2+}/F6P/P_i (26). Hence, improved catalysis comes from a more stable transition state in the presence of K^+.

Previous work of Lipscomb and co-workers (27) focused on the association of Tl^+ and K^+ with FBPase in the absence of divalent cations and/or in the presence of AMP. Under these conditions FBPase is inactive. Their investigation clearly shows the association of Tl^+ and K^+ at metal loci 1, 2, and 3, usually the observed binding sites for essential divalent activators. But how do monovalent cations interact with FBPase under conditions that support catalysis? Presented below are a series of product complexes of FBPase in the presence of Mg^{2+} and Tl^+. FBPase here is co-crystallized from an equilibrium mixture of products and reactants, containing Mg^{2+} at a saturating concentration and Tl^+ ranging from zero to 70-fold in excess of its observed K_a value. Under these conditions of crystallization FBPase is active. In the presence of Mg^{2+}, Tl^+ no longer occupies metal sites 1 and 2, but interacts at four

* This work was supported in part by National Institutes of Health Research Grant NS-10546 and National Science Foundation Grants MCB-9985565. The costs of publication of this article were defrayed in part by the payment of page charges. This article must therefore be hereby marked "*advertisement*" in accordance with 18 U.S.C. Section 1734 solely to indicate this fact.

The atomic coordinates and structure factors (code 1NUZ, 1NV0, 1NV1, 1NV2, 1NV3, 1NV4, 1NV5, 1NV6, and 1NV7) have been deposited in the Protein Data Bank, Research Collaboratory for Structural Bioinformatics, Rutgers University, New Brunswick, NJ (http://www.rcsb.org/).

‡ To whom correspondence should be addressed. Tel.: 515-294-6116; Fax: 515-294-0453; E-mail: honzatko@iastate.edu.

[1] The abbreviations used are: FBPase, fructose-1,6-bisphosphatase; F6P, fructose 6-phosphate, $F16P_2$, fructose 1,6-bisphosphate; $F26P_2$, fructose 2,6-bisphosphate; PDB, protein data bank.

sites. Two of the four sites are mutually exclusive with Mg^{2+} at site 3, whereas Tl^{+} interaction at two other sites could co-exist with Mg^{2+} at sites 1−3.

EXPERIMENTAL PROCEDURES

Materials—$F16P_2$, $F26P_2$, $NADP^+$, and AMP were purchased from Sigma. Glucose-6-phosphate dehydrogenase and phosphoglucose isomerase were from Roche Molecular Biochemicals. Other chemicals were of reagent grade or equivalent. The FBPase-deficient *Escherichia coli* strain DF657 came from the Genetic Stock Center at Yale University.

Expression and Purification of FBPase—Expression and purification of FBPase followed the procedures of Burton *et al.* (28) with minor modifications (20). *E. coli* strain DF657, deficient in FBPase, was used in order to avoid contamination of recombinant FBPase by endogenous enzyme. Protein purity and concentration was confirmed by SDS-polyacrylamide gel electrophoresis (29) and by the Bradford assay (30), respectively.

Crystallization of FBPase—Crystals of FBPase were grown by the method of hanging drops. Crystals of R-state complexes grew from equal parts of a protein solution (10 mg/ml FBPase, 10 mM KP_i, pH 7.4, 5 mM $MgCl_2$, 5 mM F6P, with or without 0.2 mM EDTA, in different concentrations of thallium acetate (0, 1, 5, 20, or 100 mM)) and a precipitant solution (100 mM Hepes pH 7.0, 5% *t*-butyl alcohol, 27% (v/v) glycerol, and 8% (w/v) polyethylene glycol 3350). Crystals of T-state complexes grew from 10 mg/ml FBPase, 10 mM KP_i, pH 7.4, 5 mM $MgCl_2$, 20 mM of thallium acetate, 5 mM F6P, and 5 mM of AMP and a precipitant solution (100 mM Hepes pH 7.0, 5% *t*-butyl alcohol, and 10% (w/v) polyethylene glycol 3350). The droplet volume was 4 μl. Wells contained 500 μl of the precipitant solution. Crystals with dimensions of 0.2 × 0.2 × 0.2 mm grew in 3 days at room temperature. Conditions of crystallization for R-state FBPase differ from those of previous studies (17, 20) and result in crystals that in some cases diffract to near atomic resolution (see below).

Data Collection—Data from FBPase complexes with 20 mM Tl^+ (T-state and R-state) were collected at synchrotron beam line X12C, Brookhaven National Laboratory, using a CCD detector developed by Brandeis University, at a temperature of 100 K. The energy (12658 eV) of x-rays coincided with the atomic absorption edge of Tl^+. Data from the crystalline complex with 1 mM of Tl^+ were collected at synchrotron beam line X4A, Brookhaven National Laboratory on an ADSC, CCD detector at a temperature of 100 K and an energy of 12658 eV. Data from the crystalline complex with 100 mM Tl^+ were collected at synchrotron beam line 14BM, APS-BioCars, Argonne National Laboratory, on an ADSC, CCD detector at a temperature of 100 K and an energy of 12658 eV. Data from complexes, co-crystallized in the presence of 0.2 mM EDTA, the 5 mM Tl^+ complex without EDTA, and the Mg^{2+} complex without Tl^+ and EDTA were collected on an R-AXIS IV^{++}/Rigaku rotating anode at a temperature of 100 K, using CuKα radiation, passed through an Osmic confocal mirror system. Data from synchrotron sources were reduced and scaled by Denzo/Scalepack (31). Data from the R-AXIS IV^{++} were processed with CrystalClear (32).

Structure Determination, Model Building, and Refinement—Crystals grown for this study are isomorphous to PDB code 1CNQ (R-state) or 1EYI (T-state). Structure determinations were initiated by molecular replacement using calculated phases from either 1CNQ or 1EYI, less ligands and water molecules. Electron density maps were calculated using CNS (33). For structures reported here, the anomalous data set was accepted only if it resulted in significant anomalous difference density at the positions of sulfur and phosphorus atoms. Modifications to structural models were done through XTALVIEW (34). Models were refined against x-ray data using CNS with force constants and parameters of stereochemistry from Engh and Huber (35). Final cycles of refinement used SHELX (36) with restraints on bonds and angle distances. The thermal parameter for Tl^+ at a specific site was fixed to the average of thermal parameters for atoms of coordinating side chains. Occupancies of Tl^+ were refined with SHELX, and confirmed in XTALVIEW against $2F_{obs}-F_{calc}$ omit maps and anomalous difference maps.

Kinetic Experiments—Assays employed the coupling enzymes, phosphoglucose isomerase and glucose-6-phosphate dehydrogenase (1). The coupling enzymes were dialyzed exhaustively in order to remove NH_4^+. Thallium acetate solutions were prepared immediately prior to their use in assays. Tl^+ up to a concentration of 15 mM had no effect on the coupling enzymes. Assays were initiated by the addition of magnesium acetate (final concentration of 5 mM), instead of magnesium chloride, to avoid the precipitation of Tl^+ by Cl^-. The concentration of $F16P_2$ in all assays was 20 μM. The reduction of $NADP^+$ to NADPH was monitored by fluorescence emission at 470 nm, using an excitation wavelength of 340 nm, as described elsewhere (23). Concentrations of Tl^+ were 0.0, 1.0, 1.5, 2.0, 2.5, 3.0, 5.0, 8.0, and 10.0 mM. All kinetic assays were performed at room temperature in triplicate. Initial rate data were fit using ENZFITTER (37). The Hill coefficient for Tl^+ activation came from a least squares fit of the following shown in Equation 1,

$$V = [V_m S^n/(K_a + S^n)] + 3.0863 \quad \text{(Eq. 1)}$$

where V is the observed initial velocity at a specific concentrations of Tl^+, S is the concentration of Tl^+, n is the Hill coefficient, K_a is the affinity constant for Tl^+, and 3.0863 is the initial velocity of the reaction in the absence of Tl^+, based upon an average of five determinations.

RESULTS

Purity of FBPase and the Influence of Tl^+ on Kinetics—FBPase used here migrates as a single band on an SDS-polyacrylamide gel and exhibits no evidence of proteolysis. A previous report regarding Tl^+-activation of FBPase from mouse liver did not provide experimental details (38) and hence the phenomenon was re-investigated here. Tl^+ does not influence the coupling enzymes of the assay system, so that the rate of formation of NADH is directly related to the rate of formation of F6P. The maximum level of Tl^+-activation for the recombinant porcine enzyme is 20%, with a Hill coefficient of 1.15 ± 0.09 and a K_a of 1.3 ± 0.1 mM. (The K_a for mouse liver enzyme is 16 mM). At Tl^+ concentrations in excess of 15 mM, the specific activity of FBPase declines. Maximal K^+-activation for the recombinant porcine enzyme under comparable assay conditions is 18% (26), with a Hill coefficient of unity and a K_a of 17 mM (13).

Quality of Crystals—Conditions of crystallization of R-state FBPase differ from those employed in past work (17, 20) in two respects: (i) $F6P_2$ replaces F6P/P_i, and (ii) glycerol is present as a cryo-protectant. Co-crystallization with substrate, rather than products, should not alter the results. The enzyme is active under the conditions of crystallization, and thus products and substrates should be at their equilibrium concentrations regardless of the starting conditions. The addition of glycerol (27%, v/v) and the reduced concentration of polyethylene glycol 3350 (from 10 to 8%, w/v), however, have resulted in an unexpected dividend. Crystals, grown in the absence of glycerol, exhibit a wide variation in x-ray diffraction properties after exposure to glycerol and rapid freezing in liquid nitrogen. Crystals soaked in glycerol are fragile and become disordered in 9 of every 10 instances. On the other hand, FBPase crystals grown in the presence of glycerol undergo rapid freezing with reproducible results. Under the new conditions of crystal growth, R-state FBPase crystals can diffract to 1.3 Å resolution (44), whereas previous crystals exhibit diffraction to 2.3 Å. The co-crystallized Tl^+ complexes reported below have a resolution limit of 1.8 Å. The reduced resolution probably arises from the combination of several distinct complexes within the same crystal that differ in their sites of Tl^+-association.

In all structures reported below, save the Tl^+/Mg^{2+}/AMP/product complex, FBPase crystallizes in the same space group (I222) and in isomorphous unit cells (Table I). The enzyme is in its R-state, with dynamic loop 52−72 in an engaged conformation, as defined previously by Zn^{2+}/product complexes (17, 20). The side chain of Tyr^{57} in the engaged conformation occupies a hydrophobic pocket (26). We observed no significant differences in the presence or absence of 0.2 mM EDTA. In the Tl^+/Mg^{2+}/AMP/product complex, FBPase adopts a T-state global conformation, with a disengaged loop 52−72 (20). As these complexes have been reported in detail in prior publications (17, 20), we focus here on changes in the active site in response to different conditions of crystal growth.

Thallium has been chosen over potassium in this study in order to detect metal binding at low occupancy. As noted above,

TABLE I
Statistics of data collection and refinement

Mg^{2+} is present in all complexes at 5 mM.

Tl^+ concentration (mM)	0[a]	1[a]	5[a]	20[a]	100[a]	1[b]	5[b]	20[b]	20[c]
Resolution limit (Å)	1.9	1.8	1.9	2.1	2	1.9	1.9	2.15	2.15
Wavelength of x-rays	1.54178	0.9795	1.5415	0.9795	0.9795	1.5415	1.5415	1.5415	0.9795
Space group	I222	I222	I222	I222	I222	I222	I222	I222	$P2_12_12$
No. of measurements	170156	238835	288138	92869	97976	182349	172612	163129	293146
No. of unique refl.	26098	30311	28039	17604	20719	26022	27106	19545	40229
Completeness of data (%):									
Overall	89.2	87.4	95.9	86.5	82.8	89	92.9	99.9	99.9
Last shell	49.2	86.8	69.9	43.7	49.2	48.8	61.3	99.1	99.9
R_{sym}[d]	0.038	0.075	0.023	0.03	0.052	0.024	0.021	0.071	0.104
No. of reflections in refinement[e]	24351	28983	26216	15652	18341	24246	25343	18552	38218
No. of atoms[f]	2723	2815	2737	2787	2689	2743	2765	2710	5519
No. of solvent sites	183	253	176	211	146	199	197	165	425
R-factor[g]	0.1927	0.2001	0.1968	0.1703	0.2042	0.1843	0.1915	0.2108	0.1824
R_{free}[h]	0.2461	0.2471	0.2559	0.2487	0.2661	0.2366	0.2453	0.2801	0.2511
Mean B (Å^2):									
Entire protein	28.2	24.6	25.8	28.2	28.6	24.8	25.8	32.6	24.4
Residues 61–69	51	50	61	96	82	51	69	94	90
Root mean square deviations:									
Bond lengths (Å)	0.007	0.008	0.007	0.006	0.006	0.007	0.007	0.006	0.006
Bond angles (degree)	1.9	1.9	1.8	1.7	1.8	1.8	1.9	1.8	1.8
Dihedral angles (degree)	25.6	24.8	24.6	24.9	25.2	25.1	25	25.3	25.7
Improper angles (degree)	1.33	1.27	1.25	1.28	1.23	1.24	1.27	1.27	1.71
Occupancies (%) of metal sites:									
Site 1, Mg^{2+}/Tl^+	100/0	84/10	95/6	58/3	0/0	80/10	75/5	78/2	100/0
Site 2, Mg^{2+}/Tl^1	100/0	100/0	68/5	50/7	100/0	80/3	82/4	60/8	0/15
Site 3, Mg^{2+}	50	10	0	0	0	40	0	0	0
Site 3a, Tl^+	0	0	11	30	33	0	13	30	15
Site 3b, Tl^+	0	0	10	18	18	4	10	17	10
Site 4, Tl^+	0	0	9	25	33	0	6	14	15
Site 5, Tl^+	0	0	10	25	35	0	9	23	14
Occupancies (%) of the 1-OH group of F6P:									
Productive	100	50	35	0	0	50	40	0	0
Nonproductive	0	50	65	100	100	50	60	100	100

[a] EDTA absent.
[b] EDTA present at 0.2 mM.
[c] EDTA absent and AMP present at 5 mM.
[d] $R_{sym} = \Sigma_j\Sigma_i|1_{ij} - \langle 1_j\rangle|/\Sigma_i\Sigma_j I_{ij}$, where i runs over multiple observations of the same intensity, and j runs over all crystallographically unique intensities.
[e] All data in the resolution ranges indicated.
[f] Includes hydrogens linked to polar atoms.
[g] R-factor $= \Sigma||F_{obs}|-|F_{calc}||/\Sigma|F_{obs}|$, $|F_{obs}| > 0$.
[h] R-factor based upon 5% of the data randomly culled and not used in the refinement.

K^+ and Tl^+ have comparable effects on the function of FBPase. The choice of wavelength here optimizes anomalous scattering from Tl^+ without introducing an anomalous signal from Mg^{2+}. At an energy of 8040 eV (λ = 1.524 Å), thallium and magnesium have f′ of −4.03 and 0.172 electrons, respectively, and f″ of 8.12 and 0.177 electrons, respectively. At an energy of 12658 eV (λ = 0.979 Å), thallium and magnesium have f′ of −18.9 and 0.0876 electrons, respectively, and f″ of 3.93 and 0.0714 electrons, respectively (41). (f′ and f″ are the real and imaginary components of anomalous scattering). On the basis of the above, magnesium contributes virtually nothing to anomalous scattering, and in fact no anomalous difference density appears at the metal-binding loci of Mg^{2+} complexes, even though distinct anomalous difference density appears at sulfur atoms (data not shown). Thallous ions bound at low fractional occupancy (0.1, for instance) may be mistaken for water molecules in electron density maps, but can be identified unambiguously in an anomalous difference map. Finally, if Mg^{2+} and Tl^+ mutually exclude each other at a binding site, then anomalous scattering data allows a direct estimate of the Tl^+ occupancy, and an indirect estimate of the Mg^{2+} occupancy at that site. Hence, the anomalous data eliminates much ambiguity in the interpretation of electron density associated with possible metal sites, and as presented below, reveals a far more complex set of interactions than had been suggested by previous studies (27).

Crystal Structure of the Mg^{2+}/Product Complex (PDB: 1NUZ)—Data from improved crystals reveal electron density at site 3 consistent with Mg^{2+} and a coordinated water molecule (Fig. 1, *top*). Asp^{68} and Glu^{97} along with two oxygen atoms of P_i complete the inner coordination shell (square pyramidal geometry) of site-3 Mg^{2+}. When assigned fractional occupancies of 0.5, thermal parameters for the Mg^{2+} and the water molecule at site 3 match those of nearby atoms of the active site. Fractional occupancies of 0.5 for residues 61−69 of dynamic loop 52−72 also result in thermal parameters that match those for other atoms of the active site. The water molecule coordinated to site-3 Mg^{2+} hydrogen bonds with the side chain of Glu^{98} and is close to the side chain of Asp^{74}. Magnesium cations at sites 2 and 3 in combination with their coordinated water molecules, P_i, Asp^{74}, Glu^{97}, and Glu^{98}, define an interconnected assembly of atoms with well defined geometry (Fig. 1). The 1-OH group of F6P coordinates the Mg^{2+} at site 1 and is in contact with the P atom of P_i (distance of separation approximately, 2.8 Å). Furthermore, the 1-O atom of F6P is equidistant (approximately, 2.7 Å) from three oxygen atoms of P_i. The angle defined by the 1-O atom of F6P, the P atom of P_i, and the remaining (distal) oxygen atom of P_i is 172°. The distal oxygen atom of P_i coordinates to Mg^{2+} at sites 2 and 3. The spatial relationships between the 1-OH group of F6P, the Mg^{2+} at site 1, and bound P_i are essentially identical to those reported in the previous Mg^{2+}/product complex (20). The Mg^{2+} at site 3 and its coordinated water molecule are probably important to the catalytic mechanism of FBPase, as discussed below.

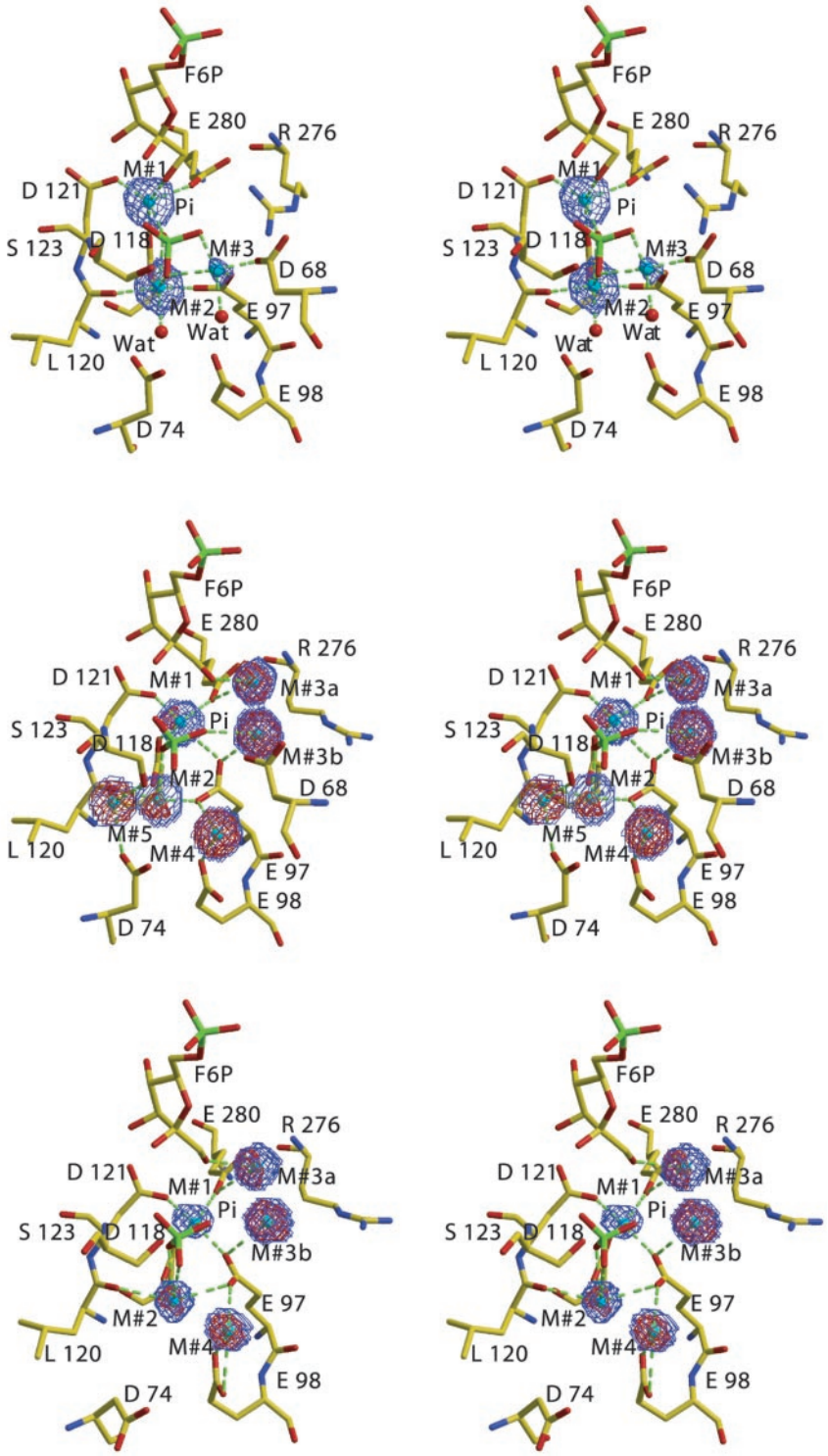

FIG. 1. **Stereoview of electron density associated with metal cations in the active site of FBPase.** The Mg^{2+}(5 mM) complex has density from a $2F_{obs}-F_{calc}$ map contoured in blue at 1σ with a cutoff radius of 1 Å (*top*). The Mg^{2+}(5 mM)/Tl^{+}(20 mM) complex has density from a $2F_{obs}-F_{calc}$ map contoured in blue at 1σ with a cutoff radius of 1 Å and density from an anomalous difference map contoured in red at 4σ with a cutoff radius of 1 Å (*middle*). The Mg^{2+}(5 mM)/Tl^{+}(20 mM)/AMP(5 mM) complex has density from a $2F_{obs}-F_{calc}$ map contoured in blue at 2σ with a cutoff radius of 1 Å and density from an anomalous difference map contoured in red at 4σ with a cutoff radius of 1 Å (*bottom*). MOLSCRIPT (40) and RASTER3D (39) were used in the preparation of this illustration.

Crystal Structure of the Tl^{+}(1 mM)/Mg^{2+}/Product Complex (PDB: 1NV0 (1NV4 with EDTA))—The addition of Tl^{+} to a concentration of 1 mM in crystallization experiments, results only in modest differences relative to the Tl^{+}-free complex. The 1-OH group of F6P now fractionally occupies two conformations, pointed toward the P-atom of P_i and away from that atom. The later conformation for the 1-OH group was observed in the Zn^{2+}/product complex (17, 20). Some anomalous difference density appears at sites 1 and 2, at positions slightly displaced from density associated with Mg^{2+} cations (Table I). The anomalous density may result from the association of Tl^{+} to active sites having no P_i. Tl^{+} cannot occupy sites 1 and 2 defined by Mg^{2+} in the presence of P_i, because of unacceptably short distances between oxygen atoms and the metal cation. Mg^{2+} remains at site 3, and a small peak of anomalous density appears at site 3a, described in detail in the following complex.

Crystal Structure of the Tl^{+}(5 mM)/Mg^{2+}/Product Complex (PDB: 1NV1 (1NV5 with EDTA))—At a concentration of 5 mM Tl^{+}, strong anomalous density appears at sites 3a, 3b, 4, and 5 (Fig. 1). Atoms that lie within 3 Å of the thallous ions are in Table II. Site 3a corresponds to site 3 of Villeret *et al.* (27). Tl^{+} at site 3a (as for sites 3b, 4, and 5) is at low occupancy (Table I). Furthermore, the fractional amount of the 1-OH group, directed away from the P-atom of P_i, has increased (Table I),

TABLE II
Metal site coordination
Listed are atoms within 2.5 Å of Mg^{2+} and 3.0 Å of Tl^+.

Coordinating residue/atom	Distance
	Å
Site 1,[a] Mg^{2+}:	
P_i O2	2.23
P_i O3	2.35
Glu^{97} OE2	2.38
Asp^{118} OD1	2.23
Asp^{121} OD1	1.92
Glu^{280} OE1	2.05
Site 2,[a] Mg^{2+}:	
P_i O2	2.01
Glu^{97} OE1	2.06
Leu^{112} O	2.30
Asp^{118} OD2	2.31
Site 3,[b] Mg^{2+}:	
P_i O3	2.49
P_i O4	2.45
Asp^{68} OD2	1.98
Glu^{97} OE2	2.19
Water	2.22
Site 3a,[a] Tl^+:	
F6P O1	3.02
Tl^+ 3b	2.69
Site 3b,[a] Tl^+:	
P_i O3	2.80
Glu^{97} OE2	2.71
Site 4,[a] Tl^+:	
Asn^{64} ND2	2.52
Glu^{98} OE2	2.77
Site 5,[a] Tl^+:	
Asp^{74} OD1	2.78
Leu^{112} O	2.70
Ser^{123} OG	2.75

[a] Mg^{2+} (5 mM)/Tl^+(20 mM) complex.
[b] Mg^{2+} (5 mM)/Tl^+(1 mM) complex.

and in fact Tl^+ at site 3a could coordinate the 1-OH group of F6P. The binding of Tl^+ to sites 3a and 3b must be mutually exclusive, as their distance of separation is only 2.5 Å. No electron density is present for Mg^{2+} at site 3, and segment 61–69 is less ordered than in the 1 mM Tl^+ complex, as evidenced by increased thermal parameters (Table I). Tl^+ at sites 3a and 3b have displaced Arg^{276} from the active site. Tl^+ at site 4 occupies the position of the water molecule, coordinated to the site-3 Mg^{2+} in the Tl^+-free complex. Tl^+ at site 5, however, coordinates the side chains of Ser^{123} and Asp^{74} without the displacement of Mg^{2+} and its coordinated water molecule from site 2. The oxygen atom of P_i, distal with respect to the 1-OH group of F6P, is 3.4 and 3.1 Å from thallous ions at sites 4 and 5, respectively, ~0.5 Å beyond that generally observed for inner-sphere coordination of Tl^+ (42).

Crystal Structures of the Tl^+(20 and 100 mM)/Mg^{2+}/Product Complex (PDB: 1NVZ (1NV6 with EDTA) and 1NV3, respectively)—The trend defined by the 1 and 5 mM Tl^+ complexes is essentially complete at a concentration of 20 mM Tl^+. Thallous cations at sites 3a, 3b, 4, and 5 do not reach full occupancy, nor does a Tl^+ concentration of 100 mM significantly increase cation levels at sites 3–5 (Table I). In fact, at 100 mM Tl^+ no metal cation occupies site 1 (Mg^{2+} is now absent). In the 20 mM Tl^+ complex, electron density is absent for segment 61–69, the 1-OH group of F6P is directed entirely away from the P-atom of P_i, and the side chain of Arg^{276} is displaced from the active site.

Crystal Structure of the Tl^+(20 mM)/Mg^{2+}/AMP Product Complex (PDB: 1NV7)—Villeret *et al.* (27) reported a Tl^+(10 mM)/AMP complex with the substrate analog 1,5-anhydroglucitol 6-phosphate. The complex reported here differs in the substitution of products for an inhibitor and the inclusion of Mg^{2+}, an essential activator of FBPase. In the complex of Villeret *et al.*, Tl^+ occupies sites 1, 2, and 3a, using our nomenclature for the metal sites in FBPase. In our complex, Mg^{2+} is at site 1, whereas Tl^+ occupies sites 2, 3a, 3b, and 4 (Fig. 1, *bottom*). Occupancy factors for all Tl^+ sites are ~0.15, but the Mg^{2+} at site 1 is at full occupancy (Table I). We observed Tl^+ at sites 3b and 4, not observed by Villeret *et al.* Reported differences in metal ligation undoubtedly arise from differences in crystallization conditions (principally the presence or absence of Mg^{2+}), but as AMP-ligated FBPase is an inhibited form of the enzyme, the functional relevance of either structure is unclear.

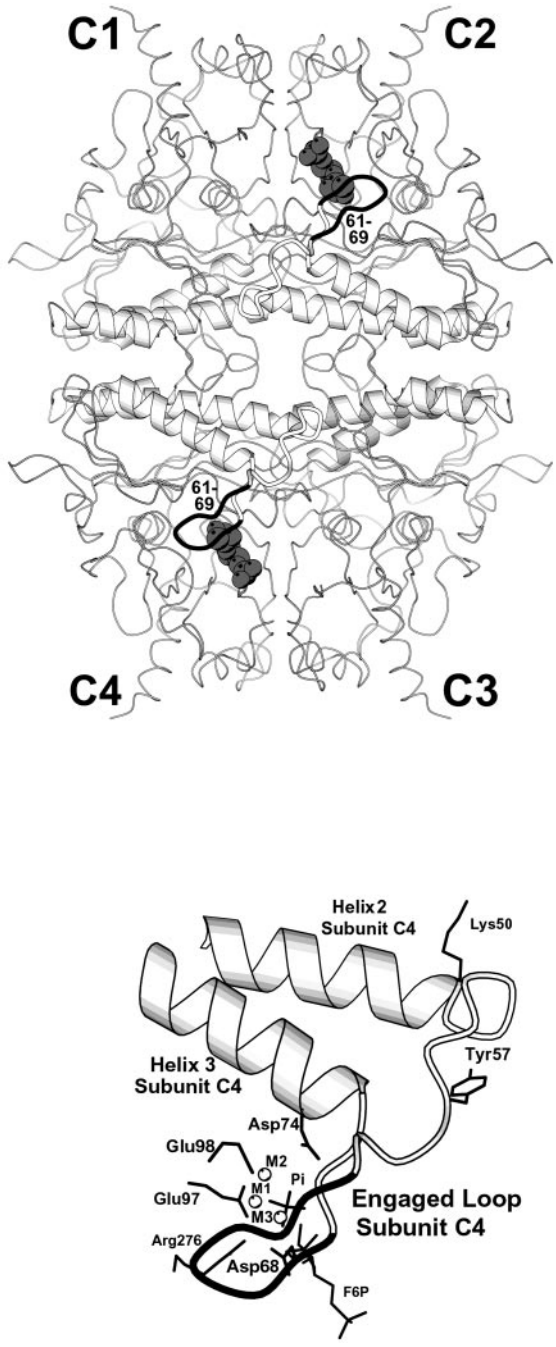

FIG. 2. **A new conformational state for loop 52–72.** The FBPase tetramer (*top*) showing the R-state, engaged loop conformation. Residues 61–69, which become disordered with increasing concentrations of Tl^+, are in *black*. *Gray spheres* represent F6P molecules. Active sites and ligands are not shown on the face of the tetramer hidden from view. A more detailed view (*bottom*) showing the proximity of residues 61–69 (main-chain ribbon in *black*) to metal binding site 3 (*M3*), P_i, and F6P. This illustration was drawn with MOLSCRIPT (40).

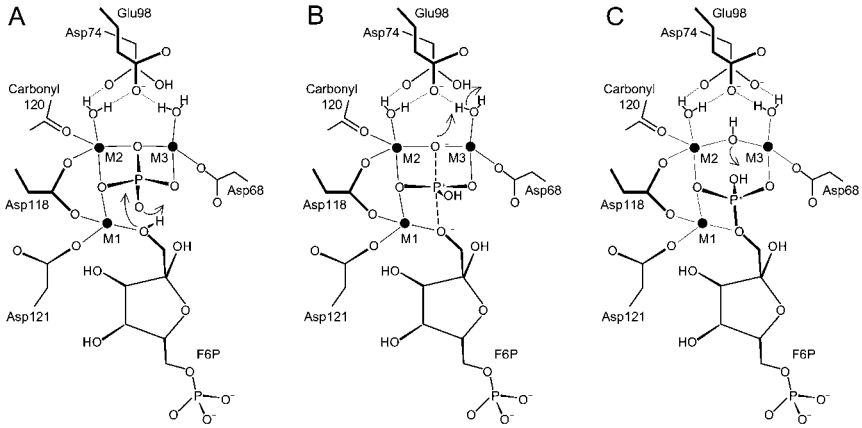

FIG. 3. **Associative mechanism for the reverse reaction of FBPase.** Glu^{280}, which coordinates to metal M1, and Glu^{97}, which coordinates metals M2 and M3, come from above the plane of the schematic, and are not shown here for clarity. *Thin*, *solid lines* are coordinate bonds, *dotted lines* represent hydrogen bonds, and *dashed lines* represent partial covalent bonds. *A*, initial product complex. The proton on Asp^{74} is hypothetical. The 1-O atom of F6P (coordinated to M1) is the attacking nucleophile. An oxygen atom of orthophosphate abstracts the proton from the 1-hydroxyl group of F6P. *B*, transition state. The leaving oxygen atom abstracts a proton from the water molecule coordinated to M3. That same water molecule in turn accepts a proton from Asp^{74}. *C*, penultimate complex. Transfer of the proton from the 1-phosphoryl group to the hydroxide anion, bridging M2 and M3, generates $F16P_2$ and water.

DISCUSSION

The presence of Mg^{2+} at site 3 is correlated with the appearance of ordered structure for segment 61–69 of the dynamic loop 52–72. The effect of Mg^{2+} at site 3 is consistent with an ordered loop in complexes that have Zn^{2+} a full occupancy at metal site 3 (17, 20). Residues 61–69 define a reverse-turn segment that lies immediately over the active site (Fig. 2). Evidently, loop 52–72 can remain in the engaged conformation (Tyr^{57} can remain in its hydrophobic pocket), while residues 61–69 cycle between a conformation that stabilizes Mg^{2+} at site 3 (by coordination to Asp^{68}) and other conformations that allow ligand exchange between the active site and bulk solvent. Mutations of Asp^{68} cause the K_a for Mg^{2+} to rise 30-fold,[2] corroborating the putative role ascribed to Asp^{68} as a chelator of a catalytically important Mg^{2+}. Hence, the transition of loop 52–72 between engaged, disordered and disengaged conformations is probably related to allosteric inhibition by AMP, whereas mobility in segment 61–69 may be important to catalytic turnover in an R-state enzyme with an engaged-loop.

The Mg^{2+} complex is consistent with an associative pathway for the hydrolysis of $F16P_2$ (Fig. 3). Magnesium ions at sites 2 and 3 coordinate the distal oxygen of P_i (the oxygen atom to be displaced by the in-line attack of the 1-OH group of F6P). Each of these magnesium cations also coordinates a water molecule, either of which could provide a proton to neutralize the negative charge on leaving oxygen atom. Glu^{98} is a proton acceptor in hydrogen bonds with both of these water molecules. Glu^{98} is required for catalysis; mutations at position 98 cause a 10,000-fold decrease in activity under conditions that support full activity of the wild-type enzyme (43). Asp^{74}, another residue essential for catalysis (24), hydrogen bonds only with the water molecule coordinated to Mg^{2+} at site 2. In fact, the oxygen atom of Asp^{74} nearest to the site-3 metal may be protonated (Fig. 3). The hydrogen atom on the 1-OH group of F6P (coordinated to site-1 Mg^{2+}) moves to an oxygen atom of the phosphate (3 oxygen atoms of P_i are all 2.7 Å from the 1-O atom of F6P). The oxygen of P_i, which hydrogen bonds with backbone amides 122 and 123, may be the most likely acceptor for the proton transferred from the 1-OH group of F6P.

Although the catalytic mechanism of Fig. 3 assumes an associative pathway for the hydrolysis of a phosphate ester, structures at near atomic resolution support the existence of metaphosphate in the active site of FBPase (44). The dissociative pathway for phosphoryl hydrolysis then is a distinct possibility, but the roles of catalytically essential side chains and the metal cations at sites 1–3 remain the same regardless of pathway.

The kinetics of monovalent cation activation is generally consistent with a simple mechanism, whereby the cation binds to a site distinct from those of the divalent cations (27, 13). Kinetic data, however, cannot exclude more complicated mechanisms, and the structures above reveal the potential for a very complex mechanism of monovalent cation activation. On the surface, the structures here agree well with the kinetics. The Hill coefficient for Tl^+-activation is 1.15, and the sum over occupancy factors for Tl^+ at sites 3–5 is 1.2. The K_a for Tl^+-activation is 1.34 mM and the sum over occupancy factors for Tl^+ sites of the 5 mM complex is approximately one-half of that at saturating levels of Tl^+. The agreement between structure and kinetics, however, may be only a coincidence. The crystallographic work here measures the binding of Tl^+ to an active site ligated by F6P and P_i, whereas the enzyme assay probes the influence of Tl^+ on a $F16P_2$-ligated active site. To the best of our knowledge, there are no reports in the literature concerning the effects of monovalent cations on the reverse reaction catalyzed by FBPase.

Each crystalline complex here represents an average of two or more states of metal ligation. The pure Mg^{2+} complex is a mixture of active sites with and without Mg^{2+} at site 3. In the Tl^+(20 mM)/Mg^{2+} complex, Mg^{2+} at site 3 and Tl^+ at sites 3b and 4 are mutually exclusive, Tl^+ at sites 3a and 3b are mutually exclusive, and metal sites 3, 3a, 3b, 4, and 5 are mutually antagonistic (occupancy factors sum to near unity; Table I). As evidenced by the Tl^+(100 mM)/Mg^{2+} complex, metal site 1 and metal sites 3a, 3b, 4, and 5 could be antagonistic as well, and in fact, inhibition by elevated concentrations of Tl^+ may arise from the displacement of Mg^{2+} from site 1.

This averaging effect in the crystal obscures the functional significance of each Tl^+ binding site, but data from Mg^{2+} complexes of FBPase at near atomic resolution provides some important insights (44). Firstly, metaphosphate/hydroxide appears in the active site of FBPase whenever the 1-OH group of F6P rotates away from its in-line orientation. We observe here the rotation of the 1-OH group away from an in-line orientation as the occupancy of Tl^+ increases at site 3a. In fact, Tl^+ at site 3a coordinates the 1-OH group and may be more effective than

[2] C. Iancu, H. J. Fromm, and R. B. Honzatko, unpublished results.

Arg^{276} in stabilizing the formation of metaphosphate in a dissociative reaction pathway. Hence, as originally suggested by Lipscomb and co-workers (27), site 3a could be a site of monovalent cation activation. On the basis of near atomic resolution data Tl^+ at site 4 coincides with an alternative binding site for Mg^{2+}. In the initial $F16P_2$ complex, Mg^{2+} may bind to site 4 and then migrate to site 3 after the formation of metaphosphate (44). Tl^+ association at site 4 may be inhibitory because of its displacement of Mg^{2+}, or Tl^+ at sites 4 and 3a together may support catalysis more effectively than Mg^{2+} at site 3 along with Arg^{276} at site 3a. Tl^+ at site 5 may not interfere with the binding of Mg^{2+} to sites 1−3. Each of the lone pair orbitals of the distal (leaving) oxygen atom of P_i, could coordinate a metal cation (Mg^{2+} at sites 2 and 3, and Tl^+ at site 5), so that an FBPase complex of Mg^{2+}(sites 1−3)/Tl^+(site 5) may be active and may exhibit enhanced catalysis.

Studies here have identified three new loci (sites 3b, 4, and 5) at the active site of FBPase for cation association in the presence of Mg^{2+}. These new sites are all within coordination distance of the substrates/products and/or amino acid residues essential to catalysis. Together these sites suggest the possibility of different pathways for the hydrolysis of $F16P_2$. Under *in vivo* conditions, however, where FBPase can select from a multitude of cations (Mg^{2+}, Mn^{2+}, Zn^{2+}, Ca^{2+}, K^+, and Li^+) at physiological concentrations and combine these cations together with products or substrate, all cation binding sites revealed here could be important in determining the net flux of reactants through gluconeogenesis.

REFERENCES

1. Krebs, H. A. (1963) in *Advances in Enzyme Regulation* (Weber, G., ed) Vol. 1, pp. 385–400, Pergamon Press Ltd., London
2. Marcus, F. (1981) in *The Regulation of Carbohydrate Formation and Utilization in Mammals* (Veneziabe, C. M., ed) pp. 269–290, University Park Press, Baltimore
3. Benkovic, S. J., and de Maine, M. M. (1982) *Adv. Enzymol. Relat. Areas Mol. Biol.* **53,** 45–82
4. Hers, H. G., and Hue, L. (1983) *Annu. Rev. Biochem.* **52,** 617–653
5. Tejwani, G. A. (1983) *Adv. Enzymol. Relat. Areas Mol. Biol.* **54,** 121–194
6. Pilkus, S. J., El-Maghrabi, M. R., and Claus, T. H. (1988) *Annu. Rev. Biochem.* **57,** 755–783
7. Taketa, K., and Pogell, B. M. (1965) *J. Biol. Chem.* **240,** 651–662
8. Nimmo, H. G., and Tipton, K. F. (1975) *Eur. J. Biochem.* **58,** 567–574
9. Stone, S. R., and Fromm, H. J. (1980) *Biochemistry* **19,** 620–625
10. McGrane, M. M., El-Maghrabi, M. R., and Pilkus, S. J. (1983) *J. Biol. Chem.* **258,** 10445–10454
11. Liu, F., and Fromm, H. J. (1988) *J. Biol. Chem.* **263,** 9122–9128
12. Sola, M. M., Oliver, F. J., Salto, R., Gutierrez, M., and Vargas, A. M. (1993) *Int. J. Biochem.* **25,** 1963–1968
13. Zhang, R., Villeret, V., Lipscomb, W. N., and Fromm, H. J. (1996) *Biochemistry* **35,** 3038–3043
14. Nimmo, H. G., and Tipton, K. F. (1975) *Eur. J. Biochem.* **58,** 575–585
15. Zhang, Y., Liang, J.-Y., Huang, S., and Lipscomb, W. N. (1994) *J. Mol. Biol.* **244,** 609–624
16. Zhang, Y., Liang, J., Huang, S., Ke, H., and Lipscomb, W. N., (1993) *Biochemistry* **32,** 1844–1857
17. Choe, J.-Y., Poland, B. W., Fromm, H. J., and Honzatko, R. B. (1998) *Biochemistry* **37,** 11441–11450
18. Ke, H., Zhang, G. Y., and Lipscomb, W. N. (1990) *Proc. Natl. Acad. Sci. U. S. A.* **87,** 5243–5247
19. Ke, H., Zhang, Y., Liang, J.-Y., and Lipscomb, W. N. (1991) *Proc. Natl. Acad. Sci. U. S. A.* **88,** 2989–2993
20. Choe, J.-Y., Fromm, H. J., and Honzatko, R. B. (2000) *Biochemistry* **39,** 8565–8574
21. Scheffler, J. E., and Fromm, H. J. (1986) *Biochemistry* **25,** 6659–6665
22. Liu, F., and Fromm, H. J. (1990) *J. Biol. Chem.* **265,** 7401–7406
23. Nelson, S. W., Kurbanov, F. T., Honzatko, R. B., and Fromm, H. J. (2001) *J. Biol. Chem.* **276,** 6119–6124
24. Kurbanov, F. T., Choe, J.-Y., Honzatko, R. B., and Fromm, H. J. (1998) *J. Biol. Chem.* **273,** 17511–17516
25. Nelson, S. W., Choe, J. Y., Honzatko, R. B., and Fromm, H. J. (2000) *J. Biol. Chem.* **275,** 29986–29992
26. Nelson, S. W., Iancu, C. V., Choe, J. Y., Honzatko, R. B., and Fromm, H. J. (2000) *Biochemistry* **39,** 11100–11106
27. Villeret, V., Huang, S., Fromm, H. J., and Lipscomb, W. N. (1995) *Proc. Natl., Acad. Sci. U. S. A.* **92,** 8916–8920
28. Burton, V. A., Chen, M., Ong, W. C., Ling, T., Fromm, H. J., and Stayton, M. M. (1993) *Biochem. Biophys. Res. Commun.* **192,** 511–517
29. Laemmli, U. K. (1970) *Nature* **227,** 680–685
30. Bradford, M. M. (1976) *Anal. Biochem.* **72,** 248–252
31. Otwinowski, Z., and Minor, W. (1997) *Methods Enzymol.* **276,** 307–326
32. CrystalClear (2001) *Rigaku Molecular Structure Corporation*, Orem, Utah
33. Brunger, A. T., Adams, P. D., Clore, G. M., DeLano, W. L., Gros, P., Grosse-Kunstleve, R. W., Jiang, J.-S., Kuszewski, J., Nilges, N., Pannu, N. S., Read, R. J., Rice, L. M., Simonson, T., and Warren, G. L. (1998) *Acta Crysallogr. Sect. D* **54,** 905–921
34. McRee, D. E. (1992) *J. Mol. Graphics* **10,** 44–46
35. Engh, R. A., and Huber, R. (1991) *Acta Crystallogr. Sect. A* **47,** 392–400
36. Sheldrick, G. M., and Gould R. O. (1995) *Acta Crystallogr. Sect. B* **51,** 423–431
37. Leatherbarrow, R. J. (1987) *ENZFITTER: A Non-Linear Regression Data Analysis Program for the IBM PC*, pp. 13–75, Elsevier Science Publishers B. V. Amsterdam.
38. Marcus, F., and Hosey, M. M. (1980) *J. Biol. Chem.* **255,** 2481–2486
39. Merritt, E. A., and Bacon, D. J. (1997) *Methods Enzymol.* **277,** 505–524
40. Kraulis, J. (1991) *J. Appl. Crystallogr.* **24,** 946–950
41. Pahler, A., Smith, J. L., and Hendrickson, W. A. (1990) *Acta Crystallogr. Sect. A* **46,** 537–540
42. Lee, A. G. (1971) *The Chemistry of Thallium*, Elsevier Publishing Company, New York
43. Kelley, N., Giroux, E. L., Lu, G., and Kantrowitz, E. R. (1996) *Biochem. Biophys. Res. Commum.* **219,** 848–852
44. Choe, J-Y., Iancu, C. V., Fromm, H. J., and Honzatko, R. B. (2003) *J. Biol. Chem.* **278,** 16015–16020

Interaction of Tl^+ with Product Complexes of Fructose-1,6-bisphosphatase

Jun-Yong Choe, Scott W. Nelson, Herbert J. Fromm and Richard B. Honzatko

J. Biol. Chem. 2003, 278:16008-16014.
doi: 10.1074/jbc.M212394200 originally published online February 20, 2003